MATHEMATICAL MODELING AND NUMERICAL SIMULATION OF A VIBRATING MEMS GYRO

Petre NEGREA[1], Constantin-Lucian SEPCU[2], Romulus LUNGU[3], Teodor Lucian GRIGORIE[4]

This paper presents theoretical and numerical study of a MEMS vibration gyro, whose operating principle is based on Coriolis effect. In a first phase is exposed the gyro mathematical modeling in terms of its dynamic regime, modeling completed during two sections with equations that describe the gyro functioning with imposed control on the excitation axis gyro controlled and mathematical implemented control on the excitation axis . The mathematical models presented are validated by numerical simulations for both considered cases: imposed control or implemented control on the excitation axis.

1. Introduction

Using integrated optics, development of quartz crystals and NEMS (Nano-electro-mechanical systems) or MEMS (Micro-electro-mechanical systems) technologies have led to significant advances in the development of miniaturized gyro systems for both highly or low precision commercial applications, and for military application. Research aimed at improving performance, miniaturization and obtaining a price able to compete with mechanical sensors. The components development and the emergence of advanced manufacturing technologies have placed the miniaturized electro-mechanical and opto-electronical sensors over the mechanical ones in terms of performance and have reduced their size to the order of a few mm^3 and even less. Initial prices were quite high, but the launch of serial production had a substantial role in diminishing those prices ([1]-[4]).

Currently, angular velocity detection with MEMS gyros uses four types of mechanisms: vibrating bars, vibrating plates, resonant rings and oscillating accelerometers. Detection is generally capacitive, but it encountered situations in which detection is on piezoresistive or piezoelectric principles. All these four

[1] PhD Student Eng., Doctoral School of Aerospace Engineering, University POLITEHNICA of Bucharest, Romania, e-mail: negreapetre@yahoo.com
[2] PhD Student, Eng., Doctoral School of Aerospace Engineering, University POLITEHNICA of Bucharest, Romania, e-mail: lsepcu@elth.ucv.ro
[3] Prof. Dr. Eng., Dept. of Electrical, Energetic and Aerospace Engineering, University of Craiova, Romania, e-mail: rlungu@elth.ucv.ro
[4] Assoc. Prof. Dr. Eng., Dept. of Electrical, Energetic and Aerospace Engineering, University of Craiova, e-mail: ltgrigorie@yahoo.com

types of gyros fall into the category of vibrating gyros. Silicon technology have enabled the development of such gyros that detects angular velocity in two or three directions simultaneously. The advantages conferred upon the strap-down inertial navigator of such gyros architectures lies in their compactness and good alignment between the measurement axes, made on micro or nano scale, which greatly reduces alignment errors of the inertial platform that appear in the situation in which are used the mono-dimensional gyros ([5]).

Reducing the size of the sensing elements has created new challenges in improving the performance of sensors, considering generally that downsizing sensors entails lower sensitivity, increased noise and decreased ability to control them. Further, the temperature varies of about 100 ppm/°C in specific Young's modulus of silicon, which causes serious problems related to thermal sensitivity.

2. Gyro dynamic equations

In Fig. 1 a) ([6]) is shown a schematic diagram of a MEMS vibrating gyro. Figure elements (seismic mass m, elastic and the damping elements) are placed in the oxy plane, solidar with the base of which the angular velocity $\vec{\Omega}$ is measured.

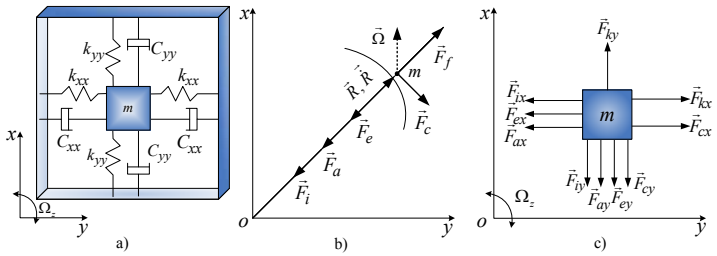

Fig. 1 Gyro schematic diagram and the specific variables

In the absence of the base rotation (Ω=0), the mass *m* is located in the origin of the coordinate system *oxyz*. When the base is rotated with the angular velocity Ω, the seismic mass m moves in a radial direction; *R* is the circumference radius and $\dot{\vec{R}}$ - radial linear velocity of the *m* mass;

$$\vec{R} = x\vec{i} + y\vec{j},\ \dot{\vec{R}} = \dot{x}\vec{i} + \dot{y}\vec{j},\ \vec{\Omega} = \Omega\vec{k}\ , \tag{1}$$

where $\vec{i}$, $\vec{j}$ and $\vec{k}$ are the axes versors of the *oxyz* frame, x and y - the current coordinates of the mass m, and $\dot{x}$ and $\dot{y}$ - the linear velocities of the mass m by the *ox* and *oy* axes directions ($\vec{R}$ components).

According to Fig. 1 b), the forces acting on the seismic mass *m* are: $\vec{F}_i$ - the inertial force, $\vec{F}_a$ - the dynamic damping force (the equivalent of the dynamic damping forces caused by the dampers as in the figure), $\vec{F}_e$ - the elastic force (the

equivalent of the elastic forces created by the elastic elements as in the figure), $\vec{F}_f$ - the centrifugal force and $\vec{F}_c$ - the Coriolis force;

$$\begin{aligned}
&\vec{F}_i = m\vec{a} = -m(a_x\vec{i} + a_y\vec{j}) = -m(\ddot{x}\vec{i} + \ddot{y}\vec{j}),\\
&\vec{F}_a = -k_a\vec{R} = -(C_{xx}\dot{x} + C_{xy}\dot{y})\vec{i} - (C_{xy}\dot{x} + C_{yy}\dot{y})\vec{j},\\
&\vec{F}_e = F_{ex}\vec{i} + F_{ey}\vec{j},\ \vec{F}_{ex} = -(k_{xx}x + k_{xy}y)\vec{i},\ \vec{F}_{ey} = -(k_{yy}y + k_{xy}x)\vec{j},\\
&\vec{F}_f = m\Omega^2\vec{R} = m\Omega^2(x\vec{i} + y\vec{j}),\\
&\vec{F}_c = -2m(\vec{\Omega}\times\dot{\vec{R}}) = \vec{F}_{cx} + \vec{F}_{cy} = -2m\Omega[\vec{k}\times(\dot{x}\vec{i} + \dot{y}\vec{j})] = 2m\Omega[(\dot{y}\vec{i} - \dot{x}\vec{j})],
\end{aligned} \tag{2}$$

where: C_{xx} and C_{yy} are the dynamic damping coefficients of the dampers, disposed by the *ox* and *oy* axes; d_{xy} - the dynamic coupling damping coefficients; k_{xx}, k_{yy} and k_{xy} are the elasticity coefficients of the elastic elements disposed by the *ox*, *oy* axes, and the coupling, respectively; $\vec{F}_{cx}$ and $\vec{F}_{cy}$ - the components of the Coriolis force by the two axes directions.

In Fig. 1 c) are given the components of the forces along the axes *ox* and *oy*; components $\vec{F}_{fx}$ and $\vec{F}_{fy}$ of the centrifugal force are small vis-à-vis of the elastic force components, being neglected; in addition, figure highlights the components $\vec{F}_{kx}$ and $\vec{F}_{ky}$ of the force $\vec{F}_k$ generated from outside, for the position control of the *m* mass (bringing mass in the neutral position, x=y=0).

The *m* mass position is obtained as a result of the balance

$$\vec{F}_i + \vec{F}_a + \vec{F}_e + \vec{F}_c + \vec{F}_k = 0. \tag{3}$$

Projecting this equation by the *ox* and *oy* axes directions, with the above expressions, is obtained the dynamic model ([7])

$$\begin{aligned}
&m\ddot{x} + C_{xx}\cdot\dot{x} + k_{xx}\cdot x + C_{xy}\dot{y} + k_{xy}\cdot y = u + 2m\Omega\dot{y},\\
&m\ddot{y} + C_{yy}\cdot\dot{y} + k_{yy}\cdot y + C_{xy}\dot{x} + k_{xy}\cdot x = -2m\Omega\dot{x},
\end{aligned} \tag{4}$$

where *m* is the vibrating mass; *x*, *y* - the proof mass coordinates with respect to the fixed frame related to the gyro housing; $u(t)$ - the electrostatic excitation force.

Relations (4) can be transfigured as

$$\begin{aligned}
&\ddot{x} + (C_{xx}/m)\cdot\dot{x} + (k_{xx}/m)\cdot x + (C_{xy}/m)\cdot\dot{y} + (k_{xy}/m)\cdot y = (u/m) + 2\Omega\dot{y},\\
&\ddot{y} + (C_{yy}/m)\cdot\dot{y} + (k_{yy}/m)\cdot y + (C_{xy}/m)\cdot\dot{x} + (k_{xy}/m)\cdot x = -2\Omega\dot{x},
\end{aligned} \tag{5}$$

and with the notations

$$\begin{aligned}
&C_{xx}/m = \omega_n/q,\ \omega_n = \sqrt{k_{xx}/m},\ C_{yy}/m = \omega_{n_1}/q_1,\ \omega_{n_1} = \sqrt{k_{yy}/m},\\
&C_{xy}/m = \omega_{n_2}/q_2,\ \omega_{n_2} = \sqrt{k_{xy}/m},\ u/m = u_c,
\end{aligned} \tag{6}$$

they became

$$\begin{aligned}\ddot{x}+(\omega_n/q)\cdot\dot{x}+\omega_n^2\cdot x+(\omega_{n2}/q_2)\cdot\dot{y}+\omega_{n2}^2\cdot y=u_c+2\Omega\dot{y},\\ \ddot{y}+(\omega_{n1}/q_1)\cdot\dot{y}+\omega_{n1}^2\cdot y+(\omega_{n2}/q_2)\cdot\dot{x}+\omega_{n2}^2\cdot x=-2\Omega\dot{x}.\end{aligned} \tag{7}$$

ω_n is the natural pulsation in the x direction; ω_{n1} - the natural pulsation in the y direction; ω_{n2} - the natural pulsation caused by coupling; q, q_1, q_2 - the quality factors on the x, y directions and coupling; u_c - the control signal on the x axis.

3. Gyro modeling with imposed control on the excitation axis

There are several types of vibrating MEMS gyros, where the proof mass trajectories in both motion directions, detection and excitation are controlled or are not controlled. The version studied in the following ensures the seismic mass trajectory control only in the x direction of excitation ([8]). Usually, to have angular velocity signal on y detection axis by Coriolis effect, the seismic mass is engaged in an oscillatory motion on x axis, according to the relation

$$x_d = A\cdot\sin\omega_n t, \tag{8}$$

where x_d is the imposed coordinate for x direction, and A is the amplitude of the imposed oscillation. So, it results

$$\dot{x}_d = A\omega_n\cos\omega_n t \tag{9}$$

and

$$\ddot{x}_d = -A\omega_n^2\sin\omega_n t. \tag{10}$$

In the situation where it is considered that the seismic mass trajectory along the x axis is controlled ($x=x_d$) and neglecting the coupling between the two axes of the system (C_{xy} =0, k_{xy}=0), the equation of motion of the seismic mass along the detection axis becomes

$$\ddot{y}+(\omega_{n1}/q_1)\cdot\dot{y}+\omega_{n1}^2\cdot y=-2\Omega\dot{x}_d, \tag{11}$$

i.e.

$$\ddot{y}+(\omega_{n1}/q_1)\cdot\dot{y}+\omega_{n1}^2\cdot y=-2\Omega\cdot A\omega_n\cdot\cos\omega_n t. \tag{12}$$

Equation (12) stationary regime solution describes the oscillator motion after the external harmonic force acted a very long time in comparison to the oscillator time constant $\tau=q_1/\omega_{n1}$ ([9]). In this case, the "transient oscillations", which describe the oscillator behavior over a period equal to few time constants, after the application of the initial external excitation, were completely extinguished. The oscillator performs then harmonics with external excitation frequency $\omega_n/2\pi$. The oscillations amplitude is proportional to the amplitude "$-2\Omega\cdot A\omega_n$" of the external excitation. Stationary solution $y_s(t)$ can be written in the form ([9])

$$y_s(t) = A_{ab}\sin\omega_n t + A_{el}\cos\omega_n t, \tag{13}$$

where A_{ab} is called the absorptive amplitude, and A_{el} is the elastic amplitude (sometimes called the dispersive amplitude);

$$A_{ab} = -2\Omega A\omega_n \cdot \frac{\omega_n \cdot (\omega_{n1}/q_1)}{\left[(\omega_{n1}^2 - \omega_n^2)^2 + \omega_n^2 \cdot (\omega_{n1}/q_1)^2\right]},$$
$$A_{el} = -2\Omega A\omega_n \cdot \frac{\omega_{n1}^2 - \omega_n^2}{\left[(\omega_{n1}^2 - \omega_n^2)^2 + \omega_n^2 \cdot (\omega_{n1}/q_1)^2\right]}. \quad (14)$$

Note that the amplitude of the harmonics contain information of angular velocity Ω. Measurement of this amplitude resort in the achievement of a demodulation with synchronous detection, as shown in Fig. 2.

This means that the signal $y(t)$ must be multiplied by $\cos\omega_n t$, i.e. with a signal containing the base harmonic of the carrier signal. Therefore, the multiplied signal becomes

$$y_d(t) = A_{ab}\sin\omega_n t\cos\omega_n t + A_{el}\cos^2\omega_n t = (A_{ab}/2)\sin 2\omega_n t + (A_{el}/2)(1+\cos 2\omega_n t). \quad (15)$$

After filtering with a low pass filter, the components with variable harmonic are cut off and remains only the continuous component, which with (14) becomes

$$y_f = \frac{A_{el}}{2} = \frac{-A\omega_n(\omega_{n1}^2 - \omega_n^2)}{\left[(\omega_{n1}^2 - \omega_n^2)^2 + \omega_n^2 \cdot (\omega_{n1}/q_1)^2\right]}\Omega, \quad (16)$$

i.e.

$$y_f = K \cdot \Omega. \quad (17)$$

Given the dependence from equation (17), is expecting a linear static characteristic of the gyro in this simplified structure.

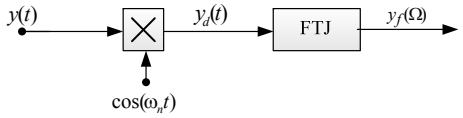

Fig. 2 Demodulation with synchronous detection

Based on the mathematical model of the simplified structure, the gyro block diagram results as in Fig. 3.

Matlab/Simulink implementation of the scheme from Fig. 3 leads to the model shown in Fig. 4. The numerical values considered for the scheme parameters are ([10]): f_n=1.58·10^5 Hz, f_{n1}=5.94·10^5 Hz, f_{n2}=1.82·10^5 Hz, m=7.55012·10^{-9} Kg, A=50 μm, q=q_1=q_2=100. f_n, f_{n1}, f_{n2} are the natural frequencies in the x, y and coupling directions, respectively.

$$\omega_n = 2\pi f_n,\ \omega_{n1} = 2\pi f_{n1},\ \omega_{n2} = 2\pi f_{n2}. \quad (18)$$

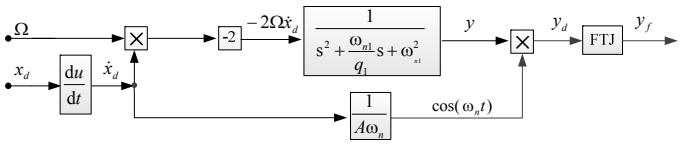

Fig. 3 Simplified gyro block diagram

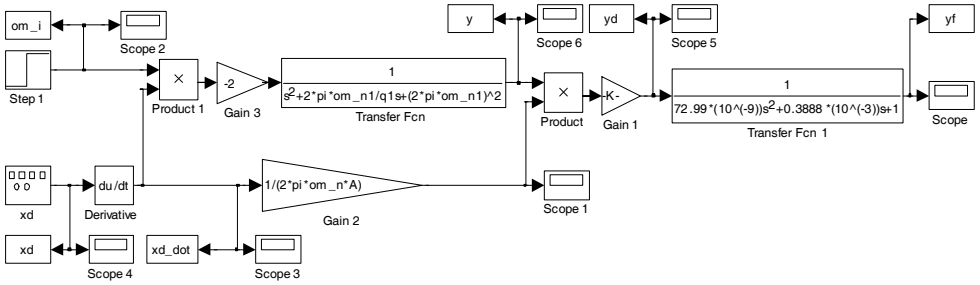

Fig. 4 The simplified gyro Matlab/Simulink model

For an angular velocity unit step input, in rad/s, the scheme signals have the allure as in Fig. 5. Can be noticed that the simulation model respects the mathematical model that it implements. The response oscillation damping is realized after approximately $2 \cdot 10^{-3}$ s, the overshoot being less than 0.04.

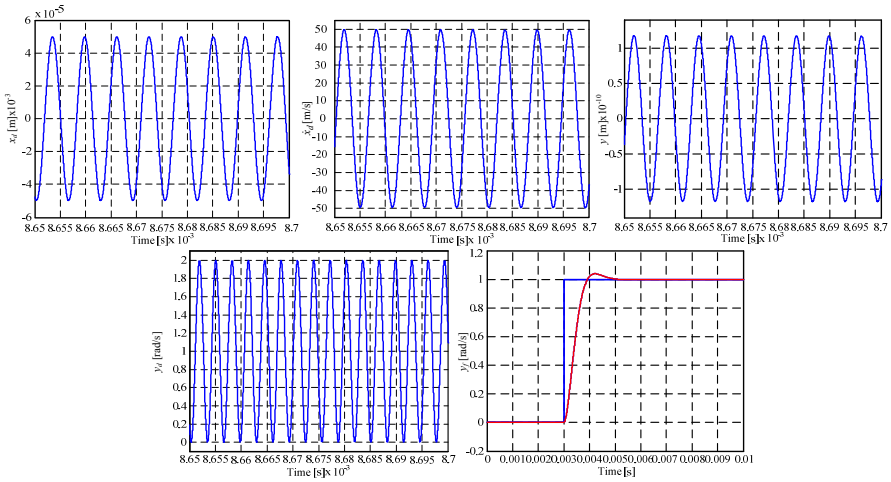

Fig. 5 Signals time variation for unit step input

To have a perfect response correlated with the input, in the simulation model scheme was added an amplification factor equal to the inverse of the scale factor K=5.8656 $\cdot 10^{-11}$.

System response to various input step can be viewed in Fig. 6, while Fig. 7 shows the gyro response to a repeated step input type. For both cases stands out a

very good behavior of the model structure and the absence of stationary error. Static characteristic of the gyro in this architecture results in the form of Fig. 8.

4. Introducing control on the excitation axis

The next study step involves placing the trajectory control on the x axis, but neglecting coupling between the two axes (C_{xy} =0, k_{xy}=0) and influence from y channel in x channel. In this case, equation (7) can be written in the form

$$\begin{aligned} &\ddot{x} + (\omega_n / q) \cdot \dot{x} + \omega_n{}^2 \cdot x = u_c, \\ &\ddot{y} + (\omega_{n1} / q_1) \cdot \dot{y} + \omega_{n1}{}^2 \cdot y = -2\Omega\dot{x}. \end{aligned} \tag{19}$$

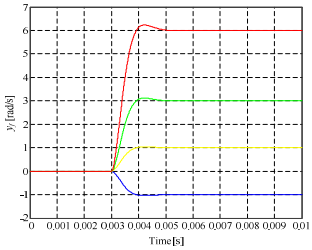

Fig. 6 Step inputs response

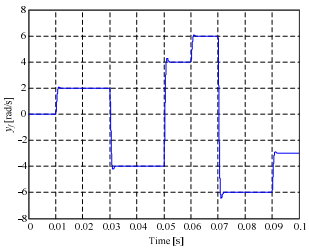

Fig. 7 Repeated step input response

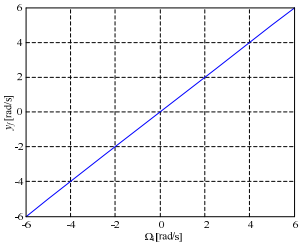

Fig. 8 Static characteristic

Choosing the control law in the following form ([10])

$$u_c = (\omega_n / q) \cdot \dot{x}_d + \omega_n^2 \cdot x_d + \nu, \tag{20}$$

with

$$\nu = -B \cdot \dot{e} - \omega_n^2 \cdot x, \tag{21}$$

first equation of (19) becomes

$$\ddot{x} + (\omega_n / q) \cdot \dot{x} + \omega_n{}^2 \cdot x = (\omega_n / q) \cdot \dot{x}_d + \omega_n^2 \cdot x_d + \nu. \tag{22}$$

e is the tracking error,

$$e = x - x_d, \tag{23}$$

and B is a parameter introduced in order to have a controlled damping in the error e dynamics ([10]).

Given the equations (8) and (10) results

$$\ddot{x}_d = -\omega_n^2 \cdot x_d, \tag{24}$$

and the expression (22) becomes

$$\ddot{x} + (-\ddot{x}_d - \omega_n^2 \cdot x_d) + (\omega_n / q) \cdot \dot{x} + \omega_n{}^2 \cdot x = (\omega_n / q) \cdot \dot{x}_d + \omega_n^2 \cdot x_d + \nu, \tag{25}$$

i.e.

$$(\ddot{x} - \ddot{x}_d) + (\dot{x} - \dot{x}_d) \cdot (\omega_n / q) + (x - x_d)\omega_n^2 = \omega_n^2 \cdot x_d + \nu, \tag{26}$$

Substituting the equations (21) and (22) into (26) is obtained

$$\ddot{e} + (\omega_n / q)\dot{e} + \omega_n^2 e = \omega_n^2 x_d - B\dot{e} - \omega_n^2 x, \tag{27}$$

The error final dynamic equation becomes

$$\ddot{e} + \left[B + (\omega_n / q)\right] \cdot \dot{e} + (\sqrt{2}\omega_n)^2 \cdot e = 0. \tag{28}$$

It has the solution in the following form ([9])

$$e(t) = e^{-t/(2\tau)} \left\{ e(0) \cdot \cos \omega_1 t + \left[\dot{e}(0) + e(0)/(2\tau)\right] \cdot (\sin \omega_1 t) / \omega_1 \right\}, \tag{29}$$

with

$$\tau = \frac{1}{(\omega_n / q) + B}, \quad \omega_1^2 = 2\omega_n^2 - \left[(\omega_n / q) + B\right]^2 / 4. \tag{30}$$

Choosing B so as $2\omega_n^2 - [(\omega_n / q) + B]^2 / 4 = \omega_1^2 > 0$ and $\tau > 0$ it results

$$\lim_{t \to \infty} e(t) = 0, \tag{31}$$

i.e.

$$\lim_{t \to \infty} x(t) = x_d(t). \tag{32}$$

With the control law in the form of (20), the system equations (19) can be rewritten in the following form

$$\begin{aligned} &\ddot{x} + (\omega_n / q) \cdot \dot{x} + \omega_n^2 \cdot x = (\omega_n / q) \cdot \dot{x}_d + \omega_n^2 \cdot x_d + \nu, \\ &\ddot{y} + (\omega_{n1} / q_1) \cdot \dot{y} + \omega_{n1}^2 \cdot y = -2\Omega \dot{x}, \\ &e = x - x_d, \\ &\nu = -B\dot{e} - \omega_n^2 x. \end{aligned} \tag{33}$$

Based on the mathematical model described by the equations (33), the gyro block diagram in Fig. 9 is obtained. The differences against the simplified model of the gyro are coming from the fact that the control, this time, is on the x axis, and the x axis input in the detection axis y is controlled by the speed $\dot{x}$ from the x axis and not through $\dot{x}_d$.

Similar to the previous situation, the model from the detection axis y corresponds to a harmonic oscillator that perform forced oscillations, with damping, produced by harmonic external excitation. Stationary regime solution in the second equation of the mathematical model of (33) describes the oscillator motion, when the transient regime for the control of variables $\dot{x}$ has fade, this motion being the source of excitation, also when the external excitation controlled $\dot{x}$, modulated in amplification with the signal -2Ω (proportional to angular velocity that has to be detected), acted a very long time compared to the time constant $\tau_1 = (q_1 / \omega_{n1})$ of the oscillator.

The detection phase modeling is described by similar equations of the model from (13)÷(17), the estimation of the angular velocity Ω being performed by synchronous detection demodulation (the scale factor is identical to the one from the situation simulated in the previous case). Implementing Fig. 9 scheme in Matlab/Simulink leads to the model shown in Fig. 10.

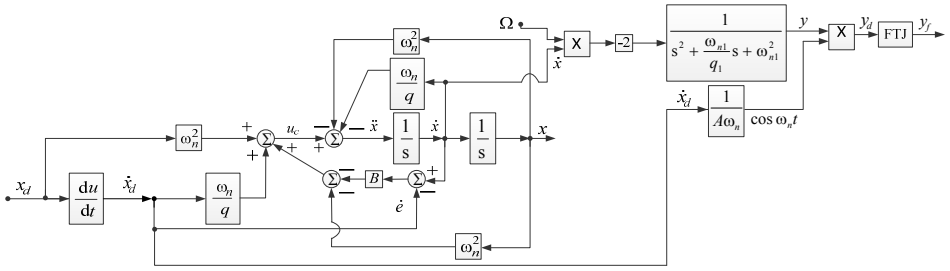

Fig. 9 Block diagram of the gyro with control on *x* axis and neglecting the two axes coupling

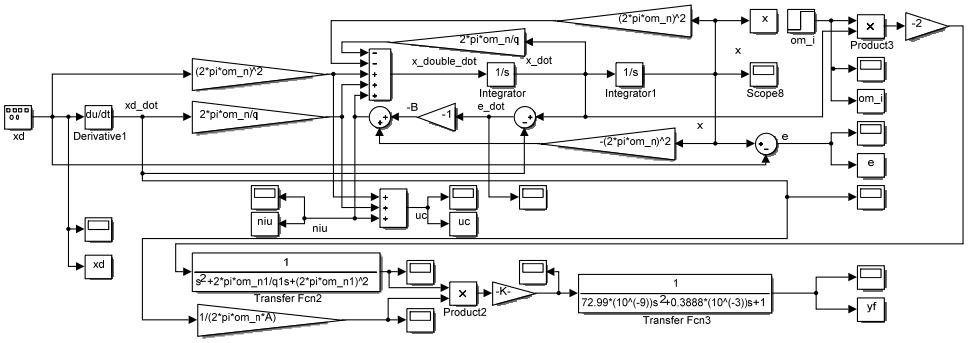

Fig. 10 Matlab/Simulink model of the gyro with control on *x* axis and neglecting the axes coupling

For a unit step input of the angular velocity Ω, in radians/s, the signals from the excitation axis have the form shown in Fig. 11, while the signals from the detection axis have the form shown in Fig. 12 (B=1was considered).

Analyzing equations (30) observes that there is an upper limit value for B that it can be increased so that $2\omega_n^2 - [(\omega_n / q) + B]^2 / 4 = \omega_1^2 \geq 0$. The time response in equation (29) suggests that τ should be as small as possible, to obtain a fastest convergence of e to 0 value. Thus, B should be chosen to have a highest value, but lower than the limit imposed by the second equation (30). It follows

$$B \leq 2\sqrt{2}\omega_n - \omega_n / q, \tag{34}$$

i.e.

$$B \leq \omega_n (2\sqrt{2} - 1/q) \cong 4.4398 \cdot 10^5. \tag{35}$$

To check the relations truthfulness that gives the approximate waveform (stationary solution) of the system from the detection y axis, i.e. equations (29), (30) and (35), the model in Fig. 10 is simulated for the following step inputs: 1, 10^2, 10^4, 10^5, $4.4398 \cdot 10^5$. The resulted characteristics of e are shown in Fig. 13. Note that numerical simulations confirm the theory, the damping optimal value of the error dynamic equation (28) being given by a value of B close to $4.4398 \cdot 10^5$.

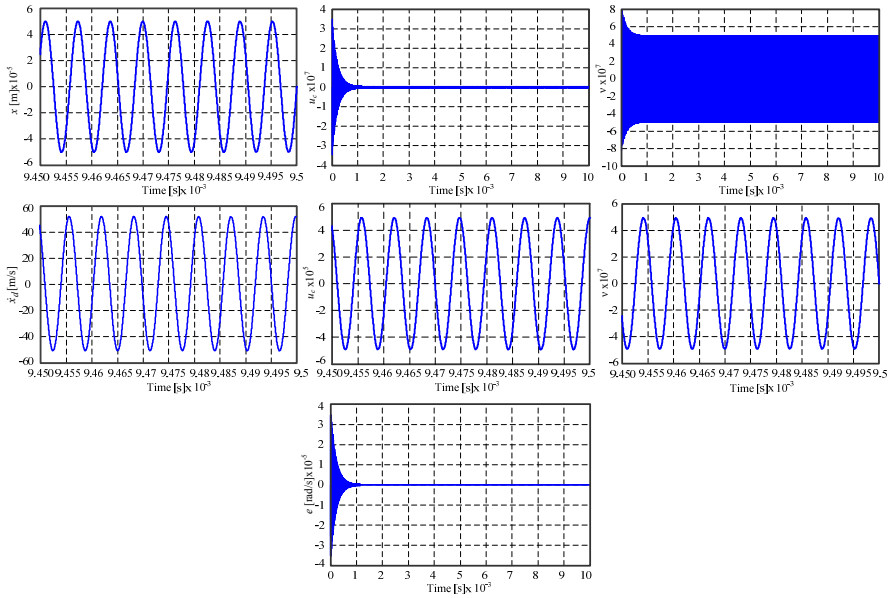

Fig. 11 Time variation of the excitation axis signals for unit step input

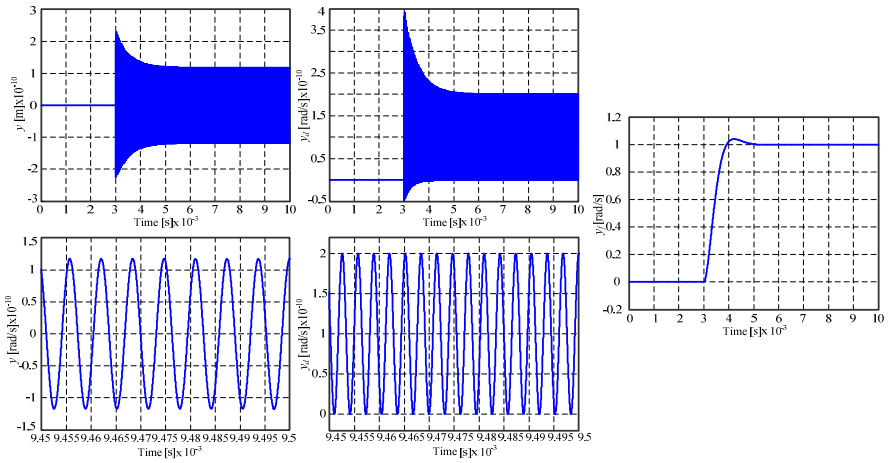

Fig. 12 Time variation of the detection axis signals for unit step input

System response to various step inputs can be viewed in Fig. 14, while Fig. 15 shows the gyro response to a repeated step input.

Can be observed that the structure in this configuration (controlled on x axis) responds very well, the obtained characteristics being similar to the simplified one. We also notice the absence of stationary error. A zoom of the $y_f(t)$ characteristic on the stationary portion shows a perfect response of the structure without parasitic oscillations. The static characteristic of the new architecture is similar to that plotted for the simplified architecture.

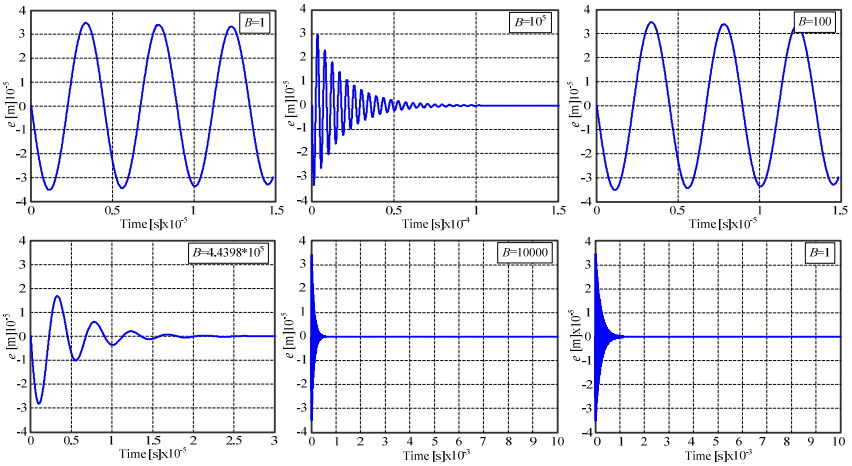

Fig. 13. Error e for different values of B

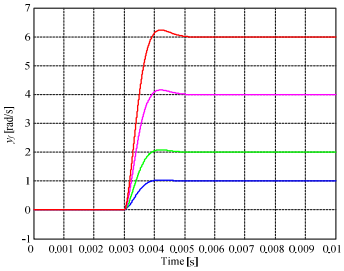

Fig. 14 Response to various step inputs

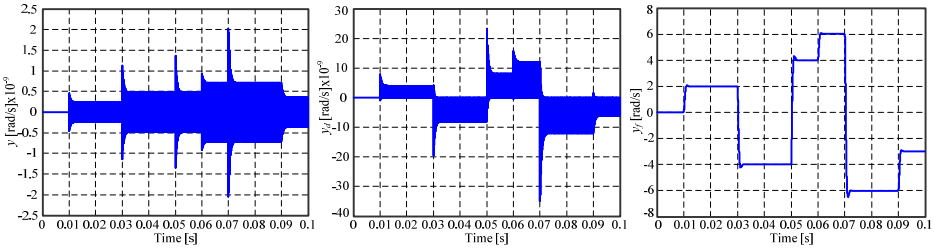

Fig. 15 Response to repeated step input

5. Conclusions

The paper presented theoretical and numerical study of a MEMS vibration gyro in two configurations: 1) with assumed control on the excitation axis (a simplified configuration used to validate the second one); 2) gyro controlled on the excitation axis. The model from the detection axis y corresponds to a harmonic oscillator performing forced oscillations, with damping, produced by harmonic external excitation, the estimation of the angular velocity Ω being performed by

synchronous detection demodulation. The first configuration assumes that the oscillation in the x axis already equals the theoretical desired one (x_d). This simplified variant was introduced in order to have a reference for the variant with the controlled oscillation in the excitation axis x to validate its modelling.

Mathematical model of the second studied architecture shown that there is an upper limit value for the damping coefficient B of the tracking error e. On the other way, the time response given by equation (29) suggested that τ should be as small as possible, to obtain a fastest convergence of e to 0 value. Thus, B should be chosen to have a highest value, but lower than the limit imposed by the second equation (30). Numerical simulations confirmed the modelling, the damping optimal value of the error dynamic equation (28) being given by a value of B closer to $4.4398 \cdot 10^5$. Also, simulations validated the mathematical model of the second configuration, showing that the obtained characteristics for controlled variables and the static characteristic are similar to the simplified configuration.

Acknowledgments

This work was supported by Romanian Space Agency (ROSA), project STAR, No. 27/19.11.2012, "High-precision micro and nano smart sensors for space inertial navigation applications", code 168/2012.

R E F E R E N C E S

[1]. *N. Barbour,* Inertial Navigation Sensors, RTO-EN-SET-116, Low-Cost Navigation Sensors and Integration Technology, March, 2010.

[2]. *N. Barbour, R. Hopkins, A. Kourepenis, P. Ward*, Inertial MEMS System Applications, NATO RTO Lecture Series, RTO-EN-SET-116, Low-Cost Navigation Sensors and Integration Technology, March, 2010.

[3]. *R. E. Hopkins., N. Barbour, D. E. Gustafson, P. Sherman*, Miniature Inertial and Augmentation Sensors for Integrated Inertial/GPS Based Navigation Applications, NATO RTO Lecture Series, RTO-EN-SET-116, Low-Cost Navigation Sensors and Integration Technology, March, 2010

[4]. *G. Schmidt*, INS/GPS Technology Trends, NATO RTO Lecture Series, RTO-EN-SET-116, Low-Cost Navigation Sensors and Integration Technology, March, 2010

[5]. *T. L. Grigorie*, Sisteme de navigatie inertiala strap-down. Studii de optimizare (Strap-down inertial navigation systems. Optimization studies). Editura Sitech, Craiova, Romania, 2007

[6]. *J. Fei, C. Batur*, Robust adaptive control for a MEMS vibratory gyroscope, Published online: 4 July 2008, Springer-Verlag London Limited 2008

[7]. *S. Park*, Adaptive control strategies for MEMS gyroscope, Ph.D. dissertation, University of California, Berkeley, 2000

[8]. *A. A. Trusov*, Overview of MEMS Gyroscopes: History, Principles of Operations, Types of Measurements, MicroSystems Laboratory, Mechanical and Aerospace Engineering University of California, Irvine, CA, 92697, USA, May 2011

[9]. *F. S. Crawford*, Waves Berkeley Physics Course vol. 3, Mcgraw-Hill College,1968

[10]. *C. Batur,* Design and control of a vibrating gyroscope, American control conference Boston, Massachusetts, 2004.